

LOCAL VERSUS GLOBAL VARIATIONAL APPROACHES TO ENHANCE WATERSHED TRANSFORMATION BASED INDIVIDUAL TREE CROWN SEGMENTATION OF DIGITAL SURFACE MODELS FROM 3K OPTICAL IMAGERY.

C. Kempf^{1,2*}, J. Tian², F. Kurz², P. d'Angelo², P. Reinartz²

¹TUM, Department of Ecology and Ecosystem Management, Freising, Germany -
{christian.kempf}@tum.de

²DLR, Department of Photogrammetry and Image Analysis, Oberpfaffenhofen, Germany -
{Jiaojiao.Tian, Franz.Kurz, Pablo.Angelo, Peter.Reinartz}@dlr.de

Commission II, WG II/3

KEY WORDS: segmentation, individual tree crown delineation, aerial stereo imagery, digital surface models

ABSTRACT:

Detection and delineation of forest trees in airborne observational data has been under study for decades, starting with images. With the advent of 3D point cloud generation techniques, much research has been spent for point cloud segmentation. From a cost perspective, aerial images are still advantageous. In this paper, two individual tree crown segmentation approaches for digital surface models are compared. Both methods attempt to enhance the drawbacks of watershed segmentation in unmanaged forests by applying a variational technique, locally to a watershed segment or globally to the image, respectively. The preprocessing by means of local histogram equalization that is necessary to harness the globally applied technique simultaneously improves the performance of the feature detection, while resulting boundaries are distorted. In contrast, the approach that uses the locally applied technique does not perform local histogram equalization prior to feature detection. It produces better localized boundaries in cases where detection is correct, but has a significantly lower rate of detection.

1. INTRODUCTION

This section describes the motivation and background of the present contribution.

1.1 Background

The problem of individual tree crown segmentation emerged in the early 90's in the analysis of areal images (Pollock, 1994), (Gougeon, 1995). It was mainly motivated by forest management tasks, such as biomass estimation. Meanwhile, the range of applications has grown considerably, also due to the availability of hyperspectral data. In particular ecological questions that are sought to be answered depend on exact knowledge of a tree's location and its boundary. Beginning in 2000, LiDaR has been used increasingly, connected with efforts to derive canopy height models (Persson et al., 2002), (Khosravipour et al., 2014). Considering acquisition costs and hence the feasible repetition rates of campaigns based on a fixed budget, optical imagery is still on the inside track. For both kinds of data, a huge amount of methods have been published. The types of forests under investigation vary, which hinders a direct comparison. An exhaustive listing is beyond the scope of the present article.

The remaining section discusses a few prominent examples that motivate the methods for digital surface model (DSM) segmentation, which are to be compared.

1.2 Related Work

(Straub, 2003) is initially carrying out a watershed segmentation (Vincent, Soille, 1991) of the squared laplacian

of the surface model at multiple scales. This is followed by topological scale-segment selection. Selected segments are then classified using also color information of corresponding RGB images. A subsequent step refines the segments using the snakes algorithm (Kass et al., 1988). Although applying the watershed transform to the squared laplacian is theoretically a good idea, in densely forested areas the inverted image gave more stable results (with the downside of boundaries in valleys). Another drawback is that trees are subjected to a strict circularity measure and the topology selection is only shape, but not surface based. Moreover, snakes can firstly only refine (can not handle topology changes) and secondly is known to be sensitive to initialization. The broader class of snakes, parametric active contours, are also prone to create cusps during the contour evolution. A similar approach can be found in (Lin et al., 2011).

(Wang et al., 2004) firstly performs laplacian of a Gaussian based edge detection with fixed mask size. Secondly, the detected grayscale maximas intersected with distance transform centres provides seedpoints for a marker controlled watershed segmentation using geodesic distances. The edge detection step is supposed to yield closed objects by supplementary thresholding of dark areas and 8-connected morphologic edge linking, which seems error-prone. Beyond that, the intersection of maximas of the grayscale image and the distance transform will exclude trees with non-centered illumination peaks.

Alternative solutions are e.g. markov random fields (Zhang, Sohn, 2010) and marked point processes (Perrin et al., 2005). Methods that are based on neural networks have only been applied to plantation-like forests or savanna trees so far (Li et al., 2009), (Zhao et al., 2018) and it seems difficult to devise a proper training strategy for unmanaged forests.

*Corresponding author

1.3 Contribution

To the best of our knowledge, more recent variational methods (specifically non-parametric active contours) have not been applied to the problem in hand. This article describes two such approaches to correct or circumvent that contours resulting from watershed segmentation on the inverted DSM are located in the middle of gaps between canopies, respectively. The first one (MCWST-MGAC) performs a marker controlled watershed transformation (MCWST) to yield segments, which may contain gap parts. The gap parts are removed by executing morphological geodesic active contours (MGAC) locally to each segment. Hence it tries to improve (Straub, 2003). The second approach (ACWE-MCWST) applies active contours without edges (ACWE), (Chan, Vese, 2001), on the global image to find an object-background separation. The subsequent watershed segmentation is then restricted to the object areas. Hence it tries to improve (Wang et al., 2004).

2. SENSOR AND DATA

This section describes the sensor system, outlines the processing chain for the generation of the DSM and presents the test data.

2.1 Sensor system

The airborne optical sensor system 3K (Leitloff et al., 2014) is composed of three Canon EOS 1Ds Mark III and provides multi-view, very high resolution (VHR) images (one nadir, two across track off-nadir). This allows to generate VHR DSMs. Details about the calibration and accuracy assessment of the camera system may be found in (Kurz et al., 2007) and (Kurz, 2009), respectively.

2.2 Processing chain

The DSM is generated by direct georeferencing. Using GNSS, images are preoriented and overlaps are found. Then SIFT features are detected, filtered using RANSAC and postprocessed using least squares adjustment. The final orientation is obtained using free bundle adjustment of the validated (SIFT-) tie points. The point cloud is calculated using semi-global matching (d'Angelo, 2016) and the DSM is derived using interpolation. These steps are integrated in the CATENA (Krauß et al., 2013) processing system.

2.3 Test data

The test data was acquired in 2016 at Kranzberg, Bavarian forest, Germany. At the flying height of 1000 m, the 3K camera system covers an area of 2560 times 480 meters with a ground sample distance of 13 cm. Three plots (deciduous, coniferous, mixed) were selected in the vicinity of the KROOF project. Figure 1 shows the RGB images and the corresponding DSMs.

The accuracy of the DSM is briefly demonstrated by visualizing marked tree tops in the image and the transformed coordinates of the DSM in figure 2. A comparison of nominal and actual transformed tree top markers shows a deviation of less than 0.5m.

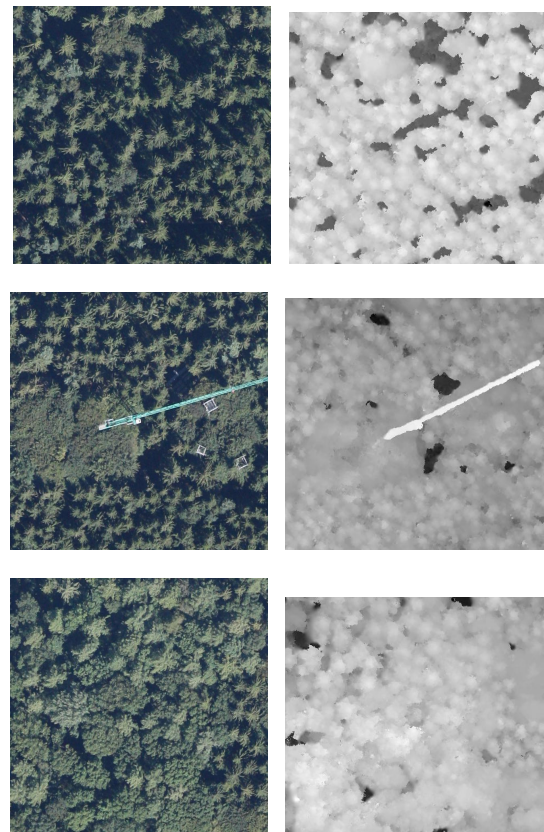


Figure 1. KROOF area: From top to bottom, the near-NADIR image / DSM of the coniferous, mixed and deciduous plots for the 3K-NIR 2016 dataset is shown in the left / right column.

3. METHODS

The two developed methods are presented in the last subsections. Each one will be outlined briefly and the single steps are explained and illustrated in more detail thereafter. Beforehand, the theory that is common to both approaches is introduced in the first subsection. The second one explains the principle of both variational techniques.

3.1 Basic methods

Blob detection A blob denotes a bright feature on dark background. In the following, it is described how such features can be detected using the Laplacian of a Gaussian (LoG).

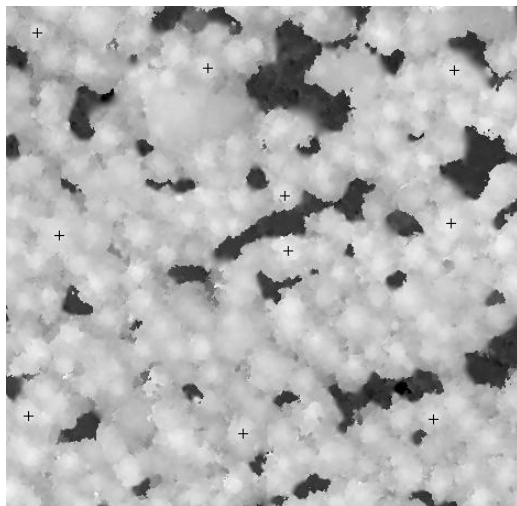
The convolution of an image f with a gaussian kernel g at different scales σ creates a scale space representation (Lindeberg, 1994), formally

$$L(x, y, \sigma) = \begin{cases} f(x, y) & , \sigma = 0 \\ g(x, y, \sigma) * f(x, y) & , \sigma > 0, \end{cases} \quad (1)$$

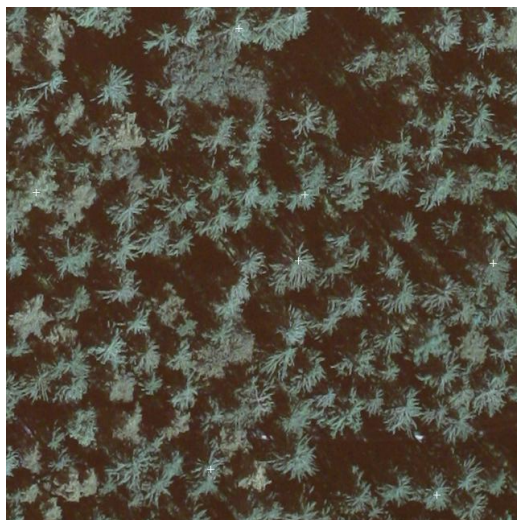
where $g(x, y, \sigma) = \frac{1}{2\pi\sigma} e^{-\frac{x+y}{2\sigma}}$. The first derivatives form the gradient operator

$$\nabla = \left(\frac{\partial}{\partial x}, \frac{\partial}{\partial y} \right). \quad (2)$$

The second derivatives form the Hessian matrix



(a) RGB



(b) DSM

Figure 2. Illustration of the transformation of manually marked point locations from the DSM to the image.

$$H = \begin{bmatrix} \frac{\partial^2}{\partial x^2} & \frac{\partial^2}{\partial xy} \\ \frac{\partial^2}{\partial xy} & \frac{\partial^2}{\partial y^2} \end{bmatrix} \quad (3)$$

H is symmetric and its principal axis representation H' exists as solution of the eigenvalue problem. The Laplace operator is defined as the trace of H' :

$$\nabla^2 = \text{trace}(H') = \frac{\partial^2}{\partial x^2} + \frac{\partial^2}{\partial y^2} \quad (4)$$

Finally, the scale normalized Laplacian of a Gaussian is defined as

$$\nabla_{norm}^2 g = \sigma \nabla^2 g. \quad (5)$$

Using $\nabla_{norm}^2 g$, a discrete 3D-laplacian scale space can be built up. A point (x, y, σ) in this scale space is identified as a blob

if it is the argument of the maximum normalized filter response among its 26 neighbours.

Watershed segmentation Intuitively, this algorithm can be regarded as a flooding simulation that starts from the minima of all catchment basins in a heightmap. A watershed line is created, where the water of neighbouring segments meets. For unseeded WST, this often leads to an oversegmentation due to spurious local minimas, created by noise. Hence, seeded WST (MCWST) uses a restricted set of minima to start the flooding process. The previously introduced Blob-LoG feature detector is one possible way to find the non-spurious minima. More details, such as the skeleton of geodesic influence zones, can be found in (Beucher, Lantuéjoul, 1979).

Curvature of surfaces The principal curvatures k_1, k_2 (minimum and maximum, respectively) and corresponding directions d_1, d_2 of a surface are calculated as the eigenvalues and corresponding eigenvectors of the Weingarten map (do Carmo, 1976). In the case of a Monge Patch, i.e. a mapping $z = f(x, y)$, the Weingarten Map coincides with the Hessian matrix. From the principal curvatures, the gaussian and mean curvatures are calculated as $G = k_1 \cdot k_2$ and $H = \frac{1}{2}(k_1 + k_2)$. In the discrete case it is essential to take into account the scale.

3.2 Variational methods

Two nonparametric active contour methods will be described. Let $C(q) : [0, 1] \rightarrow \mathbb{R}^2$ be a parametric curve (“the contour”) and let $I : [0, a] \times [0, b] \rightarrow \mathbb{R}^+$ be an image. Both methods are seeking to partition I into foreground and background and both represent the parametric curve of the object boundary as levelset (Osher, Sethian, 1988), i.e.

$$C = \{(x, y) : \phi(x, y) = 0\}, \quad (6)$$

which most significantly assures topology adaptivity. The first one is based on edge localization while the second seeks to minimize the variance among objects and background which are assumed to be constant-valued. For brevity, only the models will be presented; details of the minimization and its numerical implementation can be found in the cited references.

Morphological geodesic active contours (MGAC) (Kass et al., 1988) introduced active contours (“Snakes”) by associating a parametric curve C to the energy

$$E(C) = \alpha \int_0^1 |C'(q)|^2 dq + \beta \int_0^1 |C''(q)|^2 dq - \lambda \int_0^1 |\nabla I(C(q))| dq. \quad (7)$$

The first term is the length of the curve, the second one is its curvature. Both together can be used to enforce smoothness and are referred to as internal energy. The third term attracts the curve to edges and is called external energy. The drawbacks mentioned in the introduction were addressed in (Caselles et al., 1995). The authors point out that smoothness in equation 7 can be obtained with the first term only and the second one can thus be dropped. Furthermore they demonstrated¹ that this can be

¹This was criticized and clarified in (Aubert, Kornprobst, 2010).

transformed to the equivalent problem of computing a geodesic in Riemannian space, formally written

$$\text{Min} \int_0^1 g(|\nabla I(C(q))|) C'(q) dq, \quad (8)$$

where $s : [0, \infty) \rightarrow \mathbb{R}^+$, such that $\lim_{r \rightarrow \infty} s(r) = 0$. Without giving the details of the derivation of finding the geodesic, the boundary detection model in the levelset framework (Osher, Sethian, 1988) is stated as

$$\frac{\partial \phi}{\partial t} = s(c + \kappa) |\nabla \phi| + \nabla \phi \nabla s, \quad (9)$$

where ϕ is the levelset, t is time, κ is the curvature of the levelset and $c = \text{const.} \in \mathbb{R}^+$. A common choice for the stopping criterion g is the inverse gaussian gradient (IGG), defined as

$$s_{IGG} = \frac{1}{1 + \nabla |\hat{I}|^p} \quad (10)$$

with $p \in \{1, 2\}$ and \hat{I} the gaussian smoothed image.

Morphological computations were proven to be more stable than the use of differencing equations (Caselles et al., 1995) in (Marquez-Neila et al., 2014).

Active contours without edges (ACWE) (Chan, Vese, 2001) solve a special case of the Mumford-Shah functional, that approximates the image as piecewise continuous signal I with edges C . Here: $I(x, y) \in \{a_1, a_2\}$. The energy functional for this piecewise constant model is additively composed of a fitting term and regularization terms. The fitting term is

$$\int_{\text{inside}(C)} |I(x, y) - a_1|^2 dx dy + \int_{\text{outside}(C)} |I(x, y) - a_2|^2 dx dy, \quad (11)$$

where $a_1 = \text{average}(\{I(x, y) : I(x, y) \in \text{inside}(C)\})$, $a_2 = \text{average}(\{I(x, y) : I(x, y) \in \text{outside}(C)\})$ and C is the boundary of an open, bounded domain. The regularization terms are

$$\mu |C| + \nu \text{Area}(\text{inside}(C)), \quad (12)$$

where $|C|$ is the length of the boundary, and μ, ν are weights. The goal is to find a_1, a_2, C that minimize the sum of fitting and regularization term. C is represented as levelset function. The variational formulation requires the heavyside function

$$H(\phi) = \begin{cases} 1 & , \phi \geq 0 \\ 0 & , \phi < 0 \end{cases} \quad (13)$$

and one can rewrite:

$$|C| = \int_{\Omega} |\nabla H(\phi)| \quad (14)$$

$$\text{Area}(\text{inside}(C)) = \int_{\Omega} H(\phi) dx dy. \quad (15)$$

3.3 Local approach: MCWST-MGAC

The principle of the following approach is to find an initial segment, which is refined thereafter. The steps are illustrated in figure 3 and outlined as follows:

1. Blob detection in the DSM.
2. MCWST on the smoothed DSM using the blob centers as markers.
3. Merge small segments to its neighbour with the longest common boundary.
4. For each segment:
 - (a) Calculate a stopping criterion.
 - (b) Initialize the levelset.
 - (c) Run MGAC.

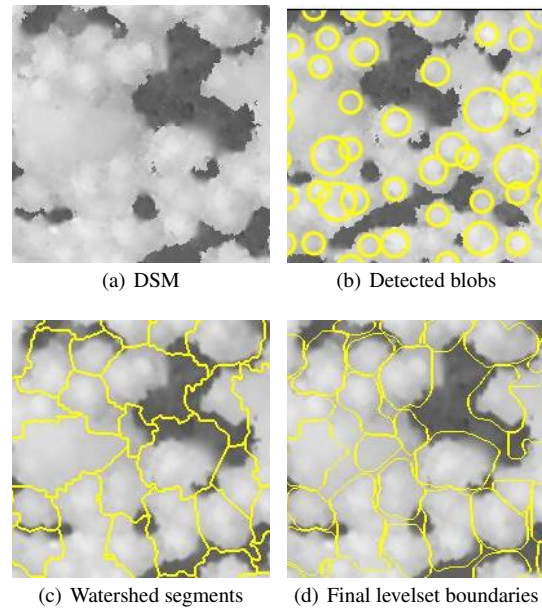


Figure 3. Illustration of the main processing steps of MCWST-MGAC.

The Blob-LoG detector requires a minimum-, maximum and step value for the scale parameter of the gaussian (cf. equation 1) to create the scale space. These are chosen to match the expected size of the trees. Furthermore, a threshold on the normalized filter response needs to be specified, which was found experimentally. At last, a maximum overlap factor can be set: when this is exceeded, smaller blobs are removed.

The DSM is smoothed with a gaussian filter of radius one prior to MCWST. The parameter for merging of small segments was set according to the smallest expected tree.

Two strategies can be pursued based on the initial watershed segmentation: Strategy 1 is to expand an initial levelset which is a contracted version of the detected blob, while the evolution should be restricted to the watershed basin. Strategy 2 is to set a negative balloon force to the contour of the watershed line. In both cases the levelset can degenerate due to missing edges, i.e. levellines that grow beyond the watershed lines or vanishing segments, respectively. In such cases a complete fallback to the watershed lines or a masking with the watershed segment can be performed, respectively.

One possibility for the stopping criterion was given in equation 10, which is suitable for the edges between canopy and ground. For throughs between trees, better results were obtained using inverse maximum principle curvature (IMPC). Both variants require a scale parameter to be specified, which is estimated by the width of the edges and throughs, respectively. Figure 3(d) shows the results using IMPC. The details of the loop are demonstrated for both variants, using two examples: In figure 4, it can be seen that the proximity to the real edge is better for IGG. Figure 5 shows that IMPC performs more reliable in transition areas of neighbouring trees.

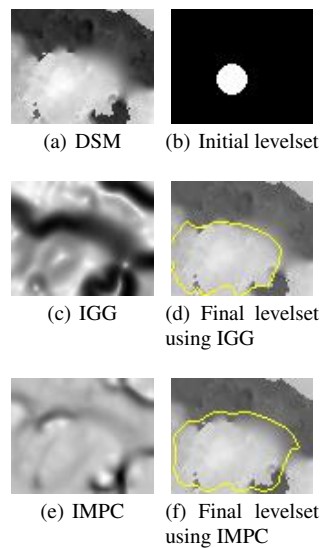


Figure 4. An example in favour of IGG.

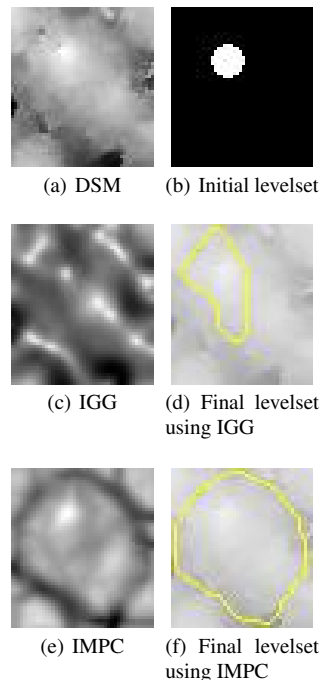


Figure 5. An example in favour of IMPC.

3.4 Global approach: ACWE-MCWST

The underlying idea here is to use an alternative, non-local method to create the object mask prior to watershed transform.

The steps are illustrated in figure 6 and can be enumerated as

1. Calculate a global threshold of the DSM.
2. Local histogram equalization (LHE) of the DSM, restricted to the areas above a fraction of the threshold.
3. Gaussian smoothing of the LHE-DSM.
4. ACWE on the smoothed LHE-DSM.
5. Blob detection on the LHE-DSM, restricted to the foreground areas of the ACWE levelset.
6. MCWST on the LHE-DSM, restricted to the foreground of the ACWE levelset, using the blob centers as markers.

The thresholding is carried out using Otsu's method (Otsu, 1979). In foreground areas of the percentile threshold mask, LHE (Gonzalez, Woods, 2001) is carried out on the DSM, with the mask size set such that it is slightly larger than the expected minimum gap between two trees. This is followed by one pass of gaussian smoothing with small $\sigma (= 1, 2)$ of the LHE-DSM. This preprocessing enables the application of ACWE to the global image resulting in a final levelset. Without LHE, the DSM violates the assumptions for the piecewise constant image model. Here, the levelset is initialized to a chessboard pattern. Blob-LoG detection is applied to the LHE-DSM, masked with the levelset foreground. Identical comments as for MGAC-MCWST apply here. The centers of the detected blob features are used as markers for the MCWST on the LHE-DSM, restricted to the object areas in the levelset.

4. EXPERIMENT

This section presents and evaluates the results of the methods introduced in the previous section. In order to accomplish the latter, the preparation of the ground truth, that corresponds to the test plots is elucidated at first.

4.1 Groundtruth

There was not enough time and personnel to carry out an inventory of the whole area. The ground truth consists of manually placed tree top markers. Ground truth boundaries are not provided for several reasons: On the one hand the DSM is partly deviating from the image. On the other hand it seems impossible to create ground truth boundaries without having a glance at the image as well. Likewise, the tree top markers were identified by visual inspection of the DSM and corresponding RGB images.

4.2 Results and accuracy assessment

Each algorithm is executed on each plot and detected trees, omission errors and commission errors are recorded. For the MCWST-MGAC approach strategy 1 was chosen and IMPC was employed. The results are displayed in figure 7 while table 1 gives the accuracy. Its evaluation avoids point in polygon testing by using the labeled DSM instead.

4.3 Discussion

The crucial factor in both methods is the blob detection, which is improved considerably using histogram equalization. For coniferous trees it is reasonable to expect a salient height maximum. For deciduous trees multiple, comparatively non-salient height maxima must be expected for a single crown or cluster of crowns. What needs to be improved

Method	Coniferous (198)	Deciduous (201)	Mixed (235)
MCWST-MGAC	188 / 155 / 43 / 34	166 / 132 / 69 / 34	197 / 166 / 69 / 31
ACWE-MCWST	205 / 179 / 19 / 26	189 / 152 / 49 / 37	210 / 177 / 58 / 33

Table 1. Each entry has the form 'segments / detections / omissions / commissions'. The total number of trees for each plot is given in the column header.

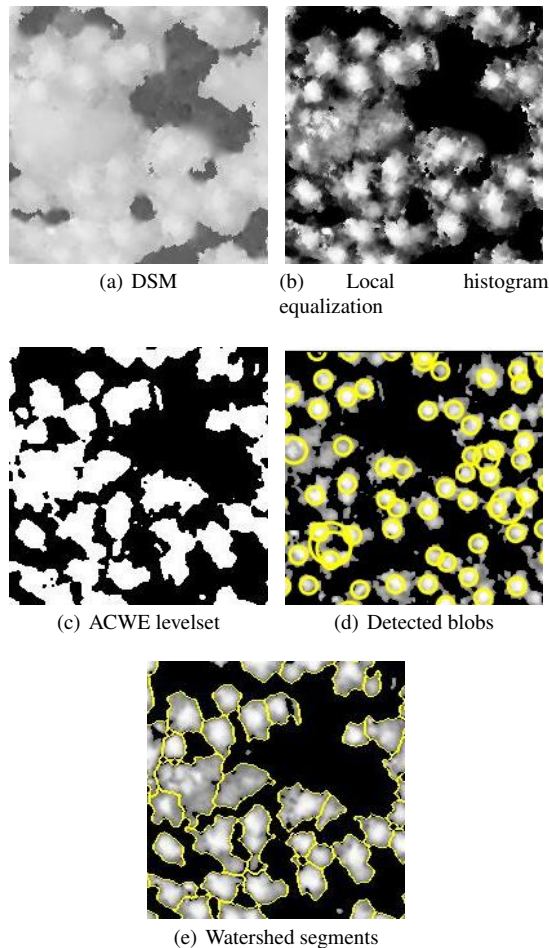


Figure 6. Illustration of the main processing steps of ACWE-MCWST.

is the ambiguity of the feature detector's response in terms of overlapping blobs for such cases. Taking into account the shape by means of the maxima of the distance transform (Felzenszwalb, Huttenlocher, 2012) can improve the result in some (e.g. trees in a row with overlap), but clearly not all cases.

Both methods accomplish to avoid, respectively correct that a tree crown boundary is located in a valley with the following downsides: ACWE-MCWST produces distorted (contracted) boundaries since it is working on the DSM after local histogram equalization. MCWST-MGAC does only produce well located boundaries if the detection has been correct, otherwise the initial levelset is likely to degenerate under expansion.

Thus, referring to deciduous trees and the actual goal to avoid distorted boundaries, a feature detection approach using the blob detector is no good choice. A straightforward attempt would be to perform blob detection on the LHE-DSM, but to execute MGAC on the original, slightly smoothed DSM. An alternative would be the use of multiphase ACWEs. This has the advantage

that no feature detection is mandatory. Still, the number of employed levelsets limits the different height sections that can be separated. Another idea is to introduce an additional surface term, that effectively encourages splitting in the case of shallow, partial gaps.

MCWST-MGAC is significantly slower than ACWE-MCWST. This seems clear because the boundary evolution is executed for each watershed segment. Since all segments are independently analyzed, there is however space for parallelization of the loop.

ACKNOWLEDGEMENTS (OPTIONAL)

This work is carried out within the project ForDroughtDet, which is funded by Waldklimafond (FKZ: 22WB410602). The authors would like to thank Thomas Schneider for discussions regarding the applications of individual tree crown segmentation.

REFERENCES

- Aubert, Gilles, Kornprobst, Pierre, 2010. *Mathematical Problems in Image Processing: Partial Differential Equations and the Calculus of Variations*. 2nd edn, Springer Publishing Company, Incorporated.
- Beucher, Serge, Lantuéjoul, Christian, 1979. Use of Watersheds in Contour Detection. <http://cmm.enscm.fr/~beucher/publi/watershed.pdf>.
- Caselles, Vicent, Kimmel, Ron, Sapiro, Guillermo, 1995. Geodesic Active Contours. *International Journal of Computer Vision*, 22, 61-79.
- Chan, T. F., Vese, L. A., 2001. Active Contours Without Edges. *Trans. Img. Proc.*, 10, 266-277. <http://dx.doi.org/10.1109/83.902291>.
- d'Angelo, Pablo, 2016. Improving semi-global matching: Cost aggregation and confidence measure. *ISPRS Congress 2016*, XLI-B1, The International Archives of the Photogrammetry, Remote Sensing and Spatial Information Sciences, 299-304.
- do Carmo, M.P., 1976. *Differential Geometry of Curves and Surfaces*. Prentice-Hall.
- Felzenszwalb, Pedro F., Huttenlocher, Daniel P., 2012. Distance Transforms of Sampled Functions. *Theory of Computing*, 8, 415-428. <http://www.theoryofcomputing.org/articles/v008a019>.
- Gonzalez, Rafael C., Woods, Richard E., 2001. *Digital Image Processing*. 2nd edn, Addison-Wesley Longman Publishing Co., Inc., Boston, MA, USA.
- Gougeon, Francois A., 1995. A Crown-Following Approach to the Automatic Delineation of Individual Tree Crowns in High Spatial Resolution Aerial Images. *Canadian Journal of Remote Sensing*, Volume 21.

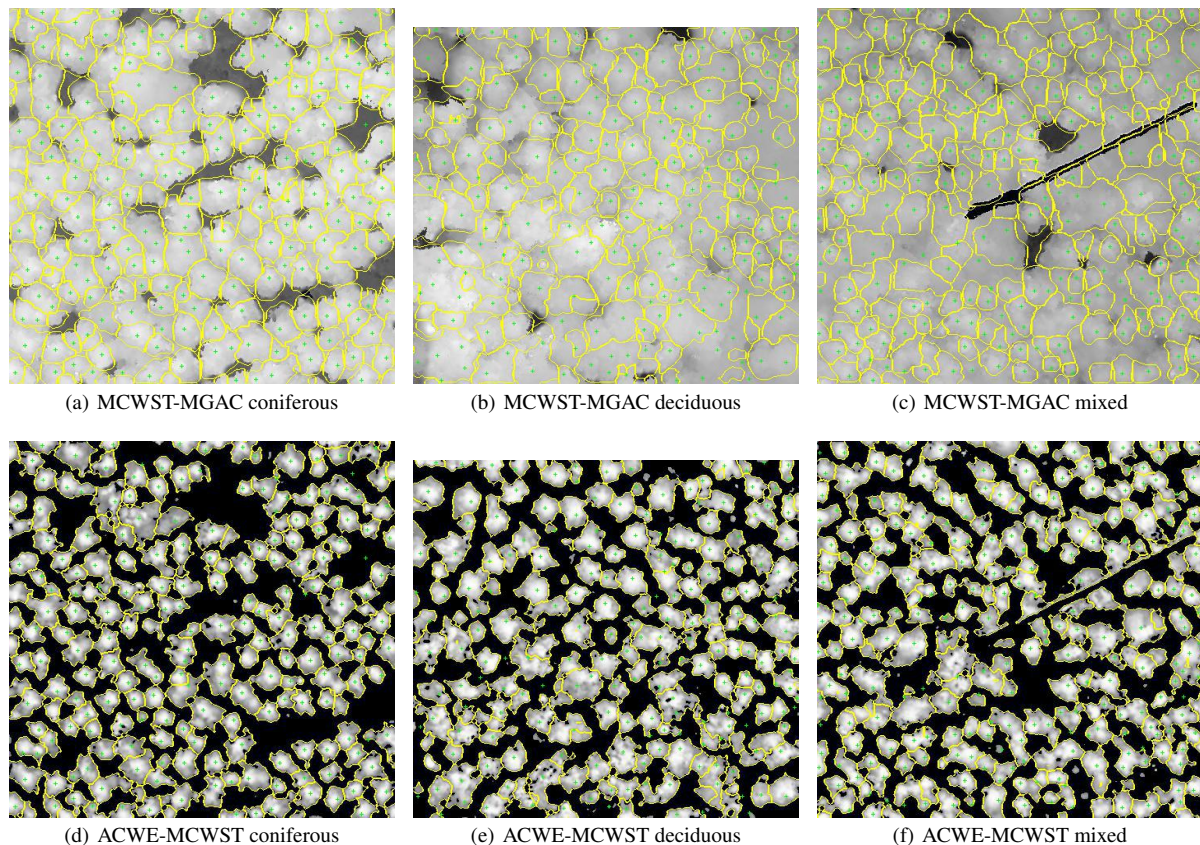


Figure 7. Segmentation results overlaid with groundtruth. The upper/lower row show the final boundaries of MCWST-MGAC / ACWE-MCWST for each of the test plots in yellow. The groundtruth tree top markers are displayed as green crosses.

Kass, Michael, Witkin, Andrew, Terzopoulos, Demetri, 1988. Snakes: Active contour models. *International Journal of Computer Vision*, 1, 321–331. <https://doi.org/10.1007/BF00133570>.

Khosravipour, Anahita, Skidmore, Andrew K, Isenburg, Martin, Wang, Tiejun, Hussin, Yousif A, 2014. Generating pit-free canopy height models from airborne lidar. *Photogrammetric Engineering & Remote Sensing*, 80, 863–872.

Krauß, T., d'Angelo, P., Schneider, M., Gstaiger, V., 2013. THE FULLY AUTOMATIC OPTICAL PROCESSING SYSTEM CATENA AT DLR. *ISPRS - International Archives of the Photogrammetry, Remote Sensing and Spatial Information Sciences*, XL-1/W1, 177–183.

Kurz, F., Müller, R., Stephani, M., Reinartz, P., Schroeder, M., 2007. Calibration of a wide-angle digital camera system for near real time scenarios. *ISPRS Hannover Workshop 2007*, The International Archives of the Photogrammetry, Remote Sensing and Spatial Information Sciences, 1682–1777.

Kurz, Franz, 2009. Accuracy assessment of the dlr 3k camera system. *DGPF Tagungsband 18 2009*.

Leitloff, Jens, Rosenbaum, Dominik, Kurz, Franz, Meynberg, Oliver, Reinartz, Peter, 2014. An Operational System for Estimating Road Traffic Information from

Aerial Images. *Remote Sensing*, 6, 11315–11341. <http://www.mdpi.com/2072-4292/6/11/11315>.

Li, Z., Hayward, R., Zhang, J., Liu, Y., Walker, R., 2009. Towards automatic tree crown detection and delineation in spectral feature space using pcnn and morphological reconstruction. *2009 16th IEEE International Conference on Image Processing (ICIP)*, 1705–1708.

Lin, Chinsu, Lo, Chein-Shun, Thomson, Gavin, 2011. A Textural Modification of the MMAC Algorithm for Individual Tree Delineation in Forest Stand using Aerial Bitmap Images. *4th International Congress on Image and Signal Processing*.

Lindeberg, Tony, 1994. *Scale-Space Theory in Computer Vision*. Kluwer Academic Publishers, Norwell, MA, USA.

Marquez-Neila, P., Baumela, L., Alvarez, L., 2014. A Morphological Approach to Curvature-Based Evolution of Curves and Surfaces. *IEEE Transactions on Pattern Analysis and Machine Intelligence*, 36, 2–17. [doi.ieeecomputersociety.org/10.1109/TPAMI.2013.106](https://doi.org/10.1109/TPAMI.2013.106).

Osher, Stanley, Sethian, James A., 1988. Fronts Propagating with Curvature Dependent Speed: Algorithms Based on Hamilton-Jacobi Formulations. *JOURNAL OF COMPUTATIONAL PHYSICS*, 79, 12–49.

Otsu, Nobuyuki, 1979. A Threshold Selection Method from Gray-Level Histograms. *IEEE Transactions*

on Systems, Man and Cybernetics, 9, 62–66.
<http://dx.doi.org/10.1109/TSMC.1979.4310076>.

Perrin, Guillaume, Descombes, Xavier, Zerubia, Josiane, 2005. *Adaptive Simulated Annealing for Energy Minimization Problem in a Marked Point Process Application*. Springer Berlin Heidelberg, Berlin, Heidelberg, 3–17.

Persson, A., Holmgren, J., Södermann, U., 2002. Detecting and measuring individual trees using an airborne laser scanner. *PERS*, 68.

Pollock, Richard J., 1994. Model-based approach to automatically locating tree crowns in high spatial resolution images. 2315, 2315 – 2315 – 12.

Straub, Bernd M., 2003. Automatic extraction of trees from aerial images and surface models. *ISPRS Archives XXXIV, Part 3/W8, Munich, 17.-19.9.2003*.

Vincent, Lee, Soill e, Pierre, 1991. Watersheds in digital spaces: An efficient algorithm based on immersion simulations. *IEEE PAMI*, 1991, 13, 583–598.

Wang, Le, Gong, Peng, Biging, Gregory S., 2004. Individual tree crown delineation and tree-top detection in high spatial resolution aerial imagery. *Photogrammetric Engineering and Remote Sensing Vol.70, Nr.3*.

Zhang, Junjie, Sohn, Gunho, 2010. A Markov Random Field Model for Individual Tree Detection from Airborne Laser Scanning Data. *IAPRS, Vol. XXXVIII, Part 3A*.

Zhao, Tiebiao, Yang, Yonghuan, Niu, Haoyu, Wang, Dong, Chen, YangQuan, 2018. Comparing u-net convolutional network with mask r-cnn in the performances of pomegranate tree canopy segmentation.

Revised 2019/04/07